ACS Catalysis

Research Article

pubs.acs.org/acscatalysis

Role of Metal–Support Interactions, Particle Size, and Metal–Metal Synergy in CuNi Nanocatalysts for H_2 Generation

Hoang Yen,[†] Yongbeom Seo,[‡] Serge Kaliaguine,[§] and Freddy Kleitz*[,†]

[†]Department of Chemistry and Centre de Recherche sur les Matériaux Avancés (CERMA), Université Laval, Quebec City G1V 0A6, Canada

[‡]Center for Nanomaterials and Chemical Reactions, Institute for Basic Science (IBS), Daejeon 305-701, Korea

[§]Department of Chemical Engineering, Université Laval, Quebec City G1V 0A6, Canada

Supporting Information

ABSTRACT: Efficient bimetallic nanocatalysts based on non-noble metals are highly desired for the development of new energy storage materials. In this work, we report a simple method for the synthesis of highly dispersed CuNi catalysts supported on mesoporous carbon or silica nanospheres using low-cost metal nitrate precursors. The mesoporous carbon-supported $Cu_{0.5}Ni_{0.5}$ nanocatalysts exhibit excellent catalytic performance for the hydrolysis of ammonia borane and decomposition of hydrous hydrazine with 100% hydrogen selectivity in aqueous alkaline solution at 60 °C. The chemical composition and size of the metal particles, which have a significant influence on the catalytic properties of the supported bimetallic CuNi materials, can readily be controlled by adjusting the metal loading and ratio of metal precursors. An exceedingly high turnover frequency of 3288 (mol_{H_2} mol_{metal}^{-1} h^{-1}) and complete reaction within 1 min in dehydrogenation of ammonia-borane were achieved over a tailored-made catalyst obtained through precise monitoring of metal particle size, composition, and support properties.

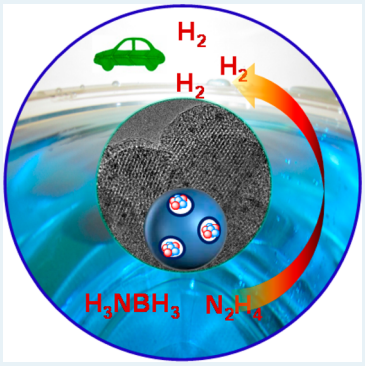

KEYWORDS: *nanocatalysts, bimetallic CuNi, synergistic effect, hydrogen generation, ammonia-borane, mesoporous nanospheres, nanoporous carbon*

INTRODUCTION

Bimetallic nanomaterials have attracted extensive theoretical and practical interest.[1−6] Catalytic properties of bimetallic nanomaterials often differ significantly from the constituent elements because of the modification of the surface geometric and electronic structures.[6−11] In addition to intrinsic changes in the bimetallic nanocatalysts brought about by composition and geometric features (e.g., particle size and shape), the electronic perturbation of the catalytic sites due to electronic metal–support interactions also has a strong influence on the inherent reactivity.[12−23] Therefore, the use of supported bimetallic nanomaterials is an interesting and important strategy for developing new catalysts with enhanced activity and selectivity. Because catalysis occurs on the surface, there are economic and fundamental incentives to produce catalysts in the form of highly dispersed supported metal nanoparticles. This could be achieved through the choice of a suitable support, the selection of proper metal precursors and the preparation method.[24−28]

On the other hand, the safe and efficient storage of hydrogen is recognized as one of the major technological barriers preventing the widespread hydrogen on-board application.[29−31] Catalyst-assisted hydrogen generation by decomposition of hydrogen storage molecules is one of the most studied and desired approaches toward a hydrogen-powered society.[32−34] Among the potential candidates for effective chemical hydrogen storage, ammonia borane (AB; NH_3BH_3) and hydrous hydrazine ($N_2H_4{\cdot}H_2O$) with high hydrogen contents have been shown to be promising hydrogen carriers for storage and transportation.[35−52] Binary metallic nanocatalysts based on the combination of noble and non-noble metals have been widely investigated for hydrogen release from both AB and hydrazine.[35−40] Although noble metal-based catalysts were shown to be effective in these reactions, the high cost hinders their widespread application, so that there is considerable current efforts devoted to explore efficient alternatives based on non-noble metals.[37,41−43] For example, bimetallic Ni–Fe, Cu–Co, Ni–Co nanoparticles were reported to be active catalysts for these reactions.[37,41,42,44,45] Nevertheless, the use of colloidal nanoparticles will raise problems of handling, stability and separation. Therefore, in the perspective of practical applications, supported metallic catalysts are preferred to avoid such problems.

Bimetallic CuNi nanocatalysts are of interest in heterogeneous catalysis for several important reactions such as methanol synthesis, water–gas shift, and steam reforming.[53−57] However, to the best of our knowledge, exploration of supported CuNi nanocatalysts in hydrogen generation from AB and hydrazine in solution has not been performed. Herein, highly active,

Received: April 28, 2015
Revised: July 3, 2015
Published: August 7, 2015

DOI: 10.1021/acscatal.5b00869
ACS Catal. 2015, 5, 5505−5511

selective and robust catalysts composed of CuNi particles supported on mesoporous carbon or silica nanospheres for hydrogen generation both from AB hydrolysis and hydrous hydrazine decomposition have now been revealed. The selected supports exhibiting mesoporous structure and spherical morphology at the nanoscale could provide high surface area for high dispersion of the catalyst nanoparticles, as well as efficient transport of the reaction agents. Among the supported CuNi catalysts tested for AB hydrolysis reaction, the mesoporous carbon-supported $Cu_{0.5}Ni_{0.5}$ catalyst exhibits the highest catalytic activity with a TOF up to 3288 (mol_{H_2} mol_{metal}^{-1} min^{-1}). Interestingly, the supported $Cu_{0.5}Ni_{0.5}$ nanocatalysts show 100% conversion of $N_2H_4.H_2O$ with 100% to H_2 selectivity at 60 °C. To gain more insight into this catalytic system, the influences of support structure, compositions, as well as the size of the metal particles, on the resulting catalyst reactivity were also substantiated.

RESULTS AND DISCUSSION

Evenly distributed CuNi nanoparticles supported on mesoporous carbon nanospheres (MCNS) with varying compositions and metal loading of 20 wt % were prepared using inexpensive nitrate metal precursors by simple incipient wetness method (see Supporting Information).

Transmission electron microscopy (TEM) and scanning TEM high-angle annular dark field (HAADF-STEM) images (Figure 1a,b and S1) clearly reveal spherical mesoporous

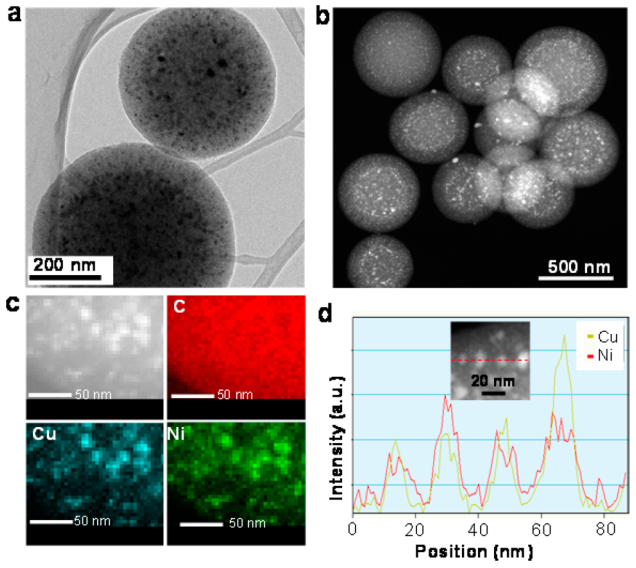

Figure 1. (a) TEM image, (b) scanning TEM high angle annular dark field (STEM-HAADF) image, and (c) the corresponding energy dispersive spectroscopy (EDS) phase mapping with (d) line-scanning profiles across the metal particles as indicated in the inset of $Cu_{0.5}Ni_{0.5}$/MCNS catalyst.

carbon particles (around 400−500 nm in size) with well-dispersed metal nanoparticles. From the TEM observations, the average particle size for the supported Ni and CuNi nanoparticles was mainly ranging from 5 to 10 nm, whereas a slightly larger particle size (13 nm) was observed for the supported Cu nanoparticles. It can be observed that the combination of Cu and Ni has a positive promoting effect on metal dispersion. The elemental analysis by energy dispersive spectroscopy (EDS) phase mappings (Figure 1c) demonstrates the uniform dispersion of Cu/Ni elements over the support. The compositional profiles of Cu and Ni along the line that is indicated in the HAADF-STEM images (Figure 1d and S1b,e) of CuNi/MCNS of different Cu/Ni ratios suggest that Cu and Ni are distributed essentially in solid solution. This feature agrees well with the X-ray diffraction (XRD) results (see below) and the signal intensities are consistent with the nominal compositions. The porosity of the prepared catalysts was confirmed by N_2 adsorption−desorption measurements. All of the samples show type IV isotherms characteristic of mesostructured materials with narrow pore size distribution centered around 3 nm (Figure S2). Textural parameters of the prepared catalysts are given in Table S1. Specific BET surface area, pore size, and pore volume of the CuNi/MCNS are quite comparable. Powder X-ray diffraction patterns (Figure 2) for CuNi/MCNS of different compositions are typical for fcc structures and the peaks can be assigned to (111) and (200) planes.

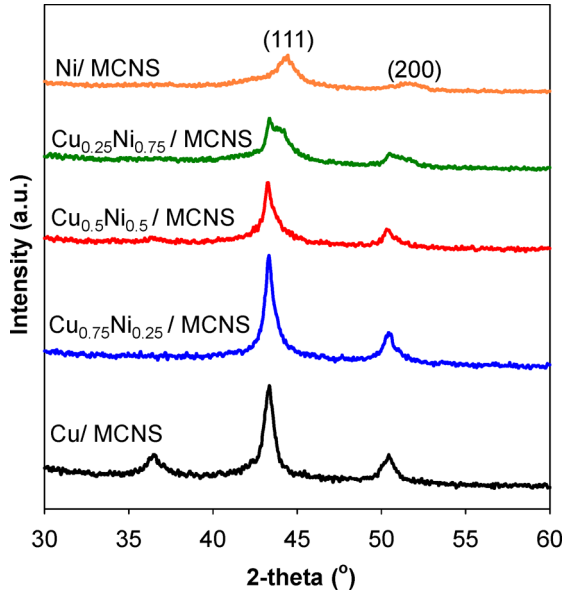

Figure 2. Wide-angle XRD patterns of catalysts with various compositions.

In the case of Cu/MCNS, one minor characteristic peak of Cu_2O at 36.4° is observed. The broad and asymmetric peaks at 2θ = 42−46° and 48−52° of the XRD patterns of bimetallic CuNi/MCNS can be resolved into two peaks corresponding to a Cu phase and a CuNi alloy phase. The chemical states of active metals in the near-surface region were obtained from XPS analyses. The XPS spectra of Cu 2p exhibit peaks mainly associated with metallic Cu^0 and Cu^+ with binding energy of Cu $2p_{3/2}$ and Cu $2p_{1/2}$ at 932.3 and 952.2 eV, respectively (Figure 3). In addition, the minor peaks located at 934.5 eV and low intensity satellites at 940−945 eV can be attributed to Cu^{2+}.[41,45,55,58] The presence of Cu^{2+} in the catalysts suggests a thin oxidized layer formed during exposure of the samples to air. Meanwhile, the XPS spectra of Ni 2p contain the main peaks attributable to Ni^{2+} with the binding energy of Ni $2p_{3/2}$ and Ni $2p_{1/2}$ at 855.5 and 872.5 eV, respectively (Figure 3).[55,58] The dominant of Ni^{2+} state in the XPS profiles indicates Ni is more susceptible to be oxidized than Cu.

Recently, catalytic hydrolysis of AB ($H_3NBH_3 + 2H_2O \rightarrow NH_4^+ + BO_2^- + 3H_2$) and decomposition of hydrazine have

DOI: 10.1021/acscatal.5b00869
ACS Catal. 2015, 5, 5505−5511

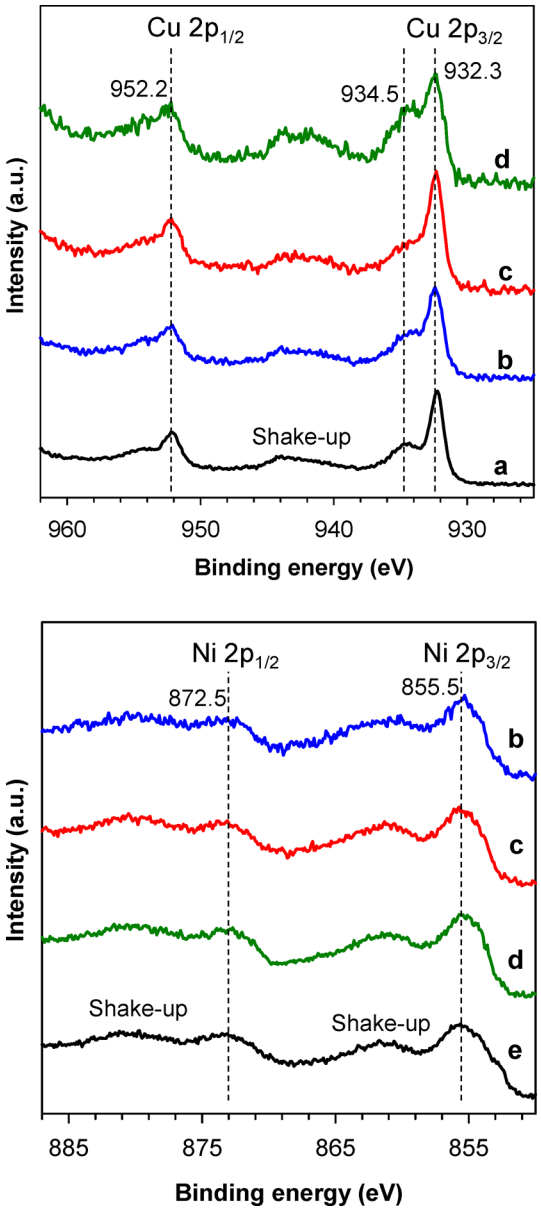

Figure 3. XPS spectra of catalysts with various compositions: (a) Cu/MCNS, (b) $Cu_{0.75}Ni_{0.25}$/MCNS, (c) $Cu_{0.5}Ni_{0.5}$/MCNS, (d) $Cu_{0.25}Ni_{0.75}$/MCNS, (e) Ni/MCNS.

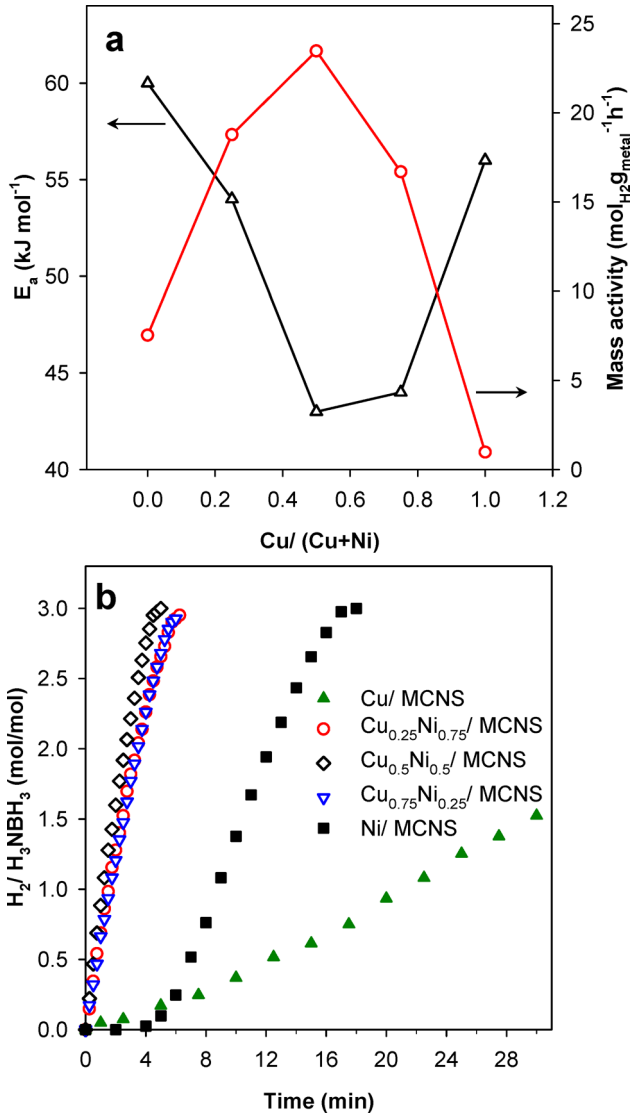

Figure 4. (a) Mass activity at 25 °C and apparent activation energy as a function of Cu molar fraction. (b) Plots of time vs volume of H_2 generated from the hydrolysis of AB catalyzed by binary CuNi/MCNS with different compositions. (H_3NBH_3 = 1.48 mmol, Metal/ [AB] = 0.036, H_2O = 10 mL, T = 25 °C).

received considerable research interest as potential approaches toward hydrogen energy-based systems.[32−34] Moreover, these processes have been used widely as adequate model reactions to study the catalytic properties of novel catalysts.[35−51]

The prepared supported CuNi nanocatalysts were first tested for the catalytic hydrolysis of AB to generate H_2 at 25−40 °C. Figure 4a shows the plots of mass activity and apparent activation energy calculated according to Arrhenius equation (Figure S3) for AB hydrolysis catalyzed by CuNi/MCNS nanocatalysts as a function of the composition. It can be observed that the activity of the catalysts strongly depends on the CuNi composition. Obviously, the H_2 generation rates of all bimetallic CuNi catalysts are greatly enhanced compared to the corresponding monometallic counterparts.

Among the tested CuNi/MCNS catalysts, $Cu_{0.5}Ni_{0.5}$ shows the highest mass activity of 23.5 mol_{H_2} g_{metal}^{-1} h^{-1}, and the dehydrogenation reaction of AB is complete within 5 min at 25 °C (Figure 4b). An induction period from 0.5 to 4 min was observed for the supported monometallic Cu and Ni catalysts, whereas gas evolution was observed to occur immediately when the catalyst was in contact with AB in the case of the bimetallic CuNi nanohybrids (Figure 4b). It has been documented that an induction period was often observed with fresh Cu- and Ni-based catalysts.[41,45,50−52] In AB hydrolysis, it is believed that the formation of an intermediate species during the induction time is essential to initiate the reaction. The formation of an activated complex is usually postulated through the interaction of an AB molecule with the surface of the solid catalyst, which then dissociates upon attack of a water molecule, releasing hydrogen.[52] Thus, the interaction between Cu and Ni here must facilitate the formation of the required activated intermediate species. The apparent activation energies for $Cu_{0.25}Ni_{0.75}$, $Cu_{0.5}Ni_{0.5}$, and $Cu_{0.75}Ni_{0.25}$/MCNS were determined to be approximately 54, 43, and 44 kJ mol^{-1}, respectively, whereas the monometallic Cu/MCNS and Ni/MCNS catalysts show higher activation energies (i.e., 56 kJ

DOI: 10.1021/acscatal.5b00869
ACS Catal. 2015, 5, 5505−5511

mol^{-1} for Cu/MCNS and 60 kJ mol^{-1} for Ni/MCNS). These results clearly indicate a catalytic synergistic effect in the hydrolysis of AB over bimetallic CuNi nanocatalysts, which is in agreement with our previous observations for nonsupported nanocast catalysts.[43]

The prepared bimetallic CuNi/MCNS catalysts were further examined in the catalytic decomposition of hydrazine. The hydrogen of hydrazine could be released by complete and desired decomposition through the pathway 1 or incomplete and undesired decomposition to ammonia by pathway 2:[34]

$$H_2NNH_2 \rightarrow N_2 + 2H_2 \text{ (pathway 1)}$$

$$3H_2NNH_2 \rightarrow 4NH_3 + N_2 \text{ (pathway 2)}$$

Pathway 2 not only decreases the yield of H_2 but also produces ammonia as a byproduct, which would poison the catalysts of hydrogen fuel cells. In our case, the prepared bimetallic CuNi/MCNS catalysts exhibit high catalytic activity in $N_2H_4{\cdot}H_2O$ decomposition for hydrogen generation in the presence of NaOH at 60 °C (Figure S4). Interestingly, all the bimetallic CuNi/MCNS catalysts showed 100% selectivity to H_2 via pathway 1 and the reaction was complete within 50 min in the case of $Cu_{0.5}Ni_{0.5}$/MCNS, whereas Cu/MCNS exhibits much lower activity and selectivity (50.5%). However, in this case, Ni/MCNS displays higher activity compared to $Cu_{0.75}Ni_{0.25}$/MCNS and Cu/MCNS. The hydrogen generation rate per unit mole of active metal over $Cu_{0.5}Ni_{0.5}$/MCNS is about 21.8 h^{-1}, which is even comparable to NiPt alloy nanoparticles.[39] It is worth noting that CuNi nanoparticles were reported to show poor activity and selectivity to H_2 (15%) at 70 °C in similar reaction conditions.[37] The improved activity and selectivity of the supported bimetallic CuNi nanocatalysts in the present work may result from a different preparation method and the type of metal precursors used, which are factors that may strongly affect the structure and properties of the catalysts. In general, surfactants and organic solvents which are frequently used in preparations of nanoparticles may remain on the catalyst surface and thus interfere in the catalytic reaction.[28,35] We have proven previously that the choice of metal precursors has a great impact on the catalyst performance in AB hydrolysis.[43] In the present case, the variation trend of activity for CuNi/MCNS catalysts with different Cu/Ni ratios was found to be similar both for AB hydrolysis and hydrazine decomposition reactions. This catalytic enhancement in both reactions and the activation energy dependence on the catalyst composition which we observed might arise from modifications of the surface electronic structure in the bimetallic nanohybrids.[10,12,15] The electronic effect on the binding strength of intermediates is due to the change in the electronic structure of a catalyst. For transition metals, the way their d-states interact with the adsorbate largely determines the binding strength. The rule is that the lower in energy the d-states are relative to the highest occupied state—the Fermi energy—of the metal, the weaker the interaction with adsorbate states due to the occupancy of antibonding states. The effect of alloying can also be understood in terms of d-band shifts. The calculated d-band centers of Cu and Ni are of −2.67 eV and −1.29 eV, respectively.[10] The d-band center position of CuNi alloy was proven to shift upward from Cu to Ni, suggesting the binding strength to CuNi bimetallic surface would lie in between Cu and Ni. Thus, the interaction between CuNi bimetallic surface and reacting species would neither be too weak nor too strong as in the cases of Cu and Ni individual systems. According to Sabatier's principle, this would explain the enhanced activity of CuNi bimetallic catalysts.[1,10,53] It was proven theoretically and experimentally that the electronic structure of a bimetallic CuNi surface can be engineered by controlling compositions, which substantially impacts the adsorbate binding energy and consequently impacts the activity and selectivity of the catalysts.[53−57,59]

In addition to composition, electronic metal−support interactions and particle size of the active components usually have a significant impact on the catalyst reactivity. Support effect and size-dependent catalytic activity of metal nanoparticles in heterogeneous catalysis are well-documented for many catalytic systems in various reactions.[12−23] It would be both of fundamental and practical interest to clarify the influence of support and particle size for the supported CuNi nanocatalysts. To do so, mesoporous silica MCM-48 and mesoporous carbon CMK-1 nanospheres were also deployed as supports,[60−62] and metal particle sizes in a range of 6.7 to 18 nm were obtained by varying the metal loading (5−20 wt %). Because the supported $Cu_{0.5}Ni_{0.5}$ nanohybrid has the highest activity among the tested catalysts, this composition was therefore applied to other supports. The ordered mesoporous structures of MCM-48 and CMK-1 nanospheres were first confirmed by low angle X-ray diffraction (Figures S5) with the reflections appearing at low 2θ angles from 1 to 6° characteristic of the $Ia3d$ structure of MCM-48 and lower symmetry $I4_132$ of the nanocast mesostructure of CMK-1.[60−62] Figure 5 and Figure S6 show typical TEM images and element mapping of $Cu_{0.5}Ni_{0.5}$/MCM-48 and $Cu_{0.5}Ni_{0.5}$/CMK-1 with various metal particle sizes. The ordered mesostructure of MCM-48 and CMK-1 supports are also clearly observed from the TEM images.

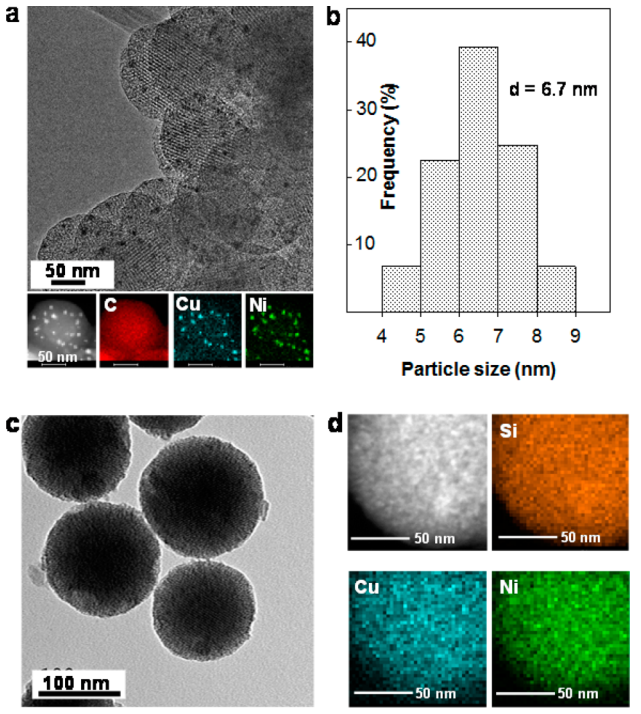

Figure 5. (a) HRTEM, STEM-HAADF images, EDS element mapping and (b) corresponding metal particle size distribution histogram of $Cu_{0.5}Ni_{0.5}$/CMK-1 with metal loading of 4.7 wt %. (c) TEM, STEM-HAADF images and (d) EDS element mapping of $Cu_{0.5}Ni_{0.5}$/MCM-48.

DOI: 10.1021/acscatal.5b00869
ACS Catal. 2015, 5, 5505−5511

The metal particles are well-dispersed with volume-averaged particle size of 6.7, 10.6, and 18 nm for $Cu_{0.5}Ni_{0.5}$/CMK-1. For $Cu_{0.5}Ni_{0.5}$/MCM-48, it can be observed that the metal particles are highly dispersed in the silica matrix. Element mapping of Cu and Ni confirms the uniform distribution of Cu and Ni for all samples. The XRD pattern of $Cu_{0.5}Ni_{0.5}$/MCM-48 (Figure S7) shows no visible peaks in the range of $2\theta = 30-60°$, suggesting the metal particles immobilized on MCM-48 nanospheres present an amorphous nature and/or are too small to be detected by XRD, in agreement with TEM observations. The visible diffraction peaks of $Cu_{0.5}Ni_{0.5}$/CMK-1 belong to the (111) and (200) planes in fcc structure of Cu and CuNi alloy phases (Figure S5). The porosity parameters obtained from the nitrogen physisorption analyses (Figure S8, 9) of the prepared catalysts are presented in Table S1. All of the mesoporous supports (MCNS, CMK-1, MCM-48) possess high specific surface area (1500−1600 m^2/g) and narrow pore size distribution in the range of 3−3.4 nm. The chemical states of Cu and Ni obtained from XPS study of $Cu_{0.5}Ni_{0.5}$/CMK-1 are similar to the $Cu_{0.5}Ni_{0.5}$/MCNS catalyst, meaning Cu, Cu^+, and Ni^{2+} coexist as main states on the surface of the catalysts. The binding energies of Cu 2p appear primarily at 932.4 and 952.5 eV, characteristic of Cu and Cu^+ (Figure S10), with an additional shoulder at 934.5 eV and low intensity of shakeup peaks indicating also the presence of Cu^{2+}. The Cu $2p_{3/2}$ and Cu $2p_{1/2}$ peaks of $Cu_{0.5}Ni_{0.5}$/MCM-48 shift slightly to higher binding energy at 932.7 and 952.5 eV compared to Cu 2p of $Cu_{0.5}Ni_{0.5}$ supported on carbon materials, indicating a larger portion of Cu^+ in the silica-supported catalyst. In addition, the low intensity shakeup peaks characteristic of Cu^{2+} can be observed. These results indicate that Cu species supported on MCM-48 are primarily in the valence state of Cu^+ and partly in the states of Cu and Cu^{2+}.

The activity of $Cu_{0.5}Ni_{0.5}$ supported on different mesoporous materials with nominal metal loading of 20 wt % were tested in AB hydrolysis. The activities of carbon-supported $Cu_{0.5}Ni_{0.5}$/CMK-1 and $Cu_{0.5}Ni_{0.5}$/MCNS catalysts are comparable (reaction completed within 2 min) and are 3-fold higher than that of the silica-supported $Cu_{0.5}Ni_{0.5}$/MCM-48 catalyst (reaction completed in 7 min) (Figure S11). Thus, one may suggest that the observed differences in activity could be associated with optimum metal particle size, electronic metal−support interactions, facilitated mass transfer, or a combination of these characteristics.

The apparent activation energy and effective reaction order can be used as simple diagnostic criteria for estimation of mass-transport limitations.[63] If the mass transfer is the rate-controlling step, the apparent activation energy is in the range of less than 5−10 kJ mol^{-1} due to the weak dependence of effective diffusivity upon temperature. According to Fick's first law, the rate of diffusion (interphase and intraparticle) is proportional to the concentration gradient (i.e., it is first order). In the case when interphase mass transfer limitations strongly dominate, a first-order of reaction is observed. Under our reaction conditions, hydrolysis catalyzed by both carbon- and silica-supported CuNi catalysts was found to be essentially independent of the AB concentration with a line slope of 0.02 and 0.07 for the silica- and carbon-supported catalysts, respectively (Figure S12). In addition, the apparent activation energy was found in the range 43−60 kJ mol^{-1} for the catalysts with different Cu/Ni ratios. Note that the particle size of the CMK-1 and MCM-48 supports are in the same range of about 150 nm, whereas the MCNS support has a larger particle size of about 400−500 nm, while the pore sizes of the catalysts are comparable. Thus, the effect of mass transfer can be viewed as negligible in our reaction systems. Therefore, the substantially higher performance of the carbon-supported catalysts originates essentially from the intrinsic activity and/or the amount of the active phases.

Interestingly, it is observed that the mean sizes of metal particles of the three catalysts are different and decrease in the order of $Cu_{0.5}Ni_{0.5}$/CMK-1 > $Cu_{0.5}Ni_{0.5}$/MCNS > $Cu_{0.5}Ni_{0.5}$/MCM-48, which means that the activity of the catalysts seems to decrease as the metal particle size decreases. In order to study the particle size dependence of the catalytic activity, three catalysts with metal average particle sizes of 6.7, 10.6, and 18 nm were obtained by using metal loading of 5, 10, and 20 wt %, respectively, using the same support, CMK-1. The CMK-1 was chosen as a support to examine the particle size effect owing to the fact that the metals supported on CMK-1 carbon exhibit a narrower particle size distribution, and, practically, the dispersion of the metal particles is also more readily visible on CMK-1. The mass activity in the catalytic AB hydrolysis increases with the decreasing metal particle sizes of the catalysts (Figure 6a and 6b). Remarkably, $Cu_{0.5}Ni_{0.5}$/CMK-1 with metal particle size of 6.7 nm shows an extremely high activity, where the hydrolysis is completed within 1 min and TOF value as high as 3288 (mol_{H_2} mol_{metal}^{-1} h^{-1}) is observed, which is superior to any other non-noble metal-based catalysts reported thus far and comparable to noble metal catalysts (Table S2)[36,48,49,51] Furthermore, the reusability tests reveal that this catalyst is still highly active after six subsequent runs of AB hydrolysis (Figure S13).

The activity normalized to theoretical surface area of the metal particles, assuming spherical nanoparticles with all the surface being catalytically available, however, decreases as the metal particle size decreases, indicating that larger particles seem more active than small ones in catalytic hydrolysis of AB under the studied conditions. To clarify this, one may consider different distribution of Cu and Ni species in the different catalytic systems under study. Indeed, the surface Ni/Cu ratio obtained from XPS analyses (Ni/Cu = 1.08/1) was found to be close to the value in the bulk determined from ICP analyses for $Cu_{0.5}Ni_{0.5}$/CMK-1 with metal particle size of 18 nm (see Table S3 in the Supporting Information). However, the catalysts show an enrichment in Ni at their surface as the metal particle size decreases; that is, the surface Ni/Cu ratios are 1.28 and 2.36 for $Cu_{0.5}Ni_{0.5}$/CMK-1 with particle sizes of 10.6 and 6.7 nm, respectively. These results suggest that the coexistence of Cu and Ni on the catalyst surface is essential to activate AB. Furthermore, we observed that $Cu_{0.5}Ni_{0.5}$/MCNS having higher metal dispersion with average particle size of 7.7 nm exhibits slightly lower reaction rate compared to $Cu_{0.5}Ni_{0.5}$/CMK-1, with mean metal particle size of 18 nm. This behavior could be explained by the fact that $Cu_{0.5}Ni_{0.5}$/MCNS is also richer in Ni on the surface, demonstrating a Ni/Cu ratio of 2.86. Therefore, the positive effect originating from increasing surface metal area due to smaller particle size can be balanced by a negative effect brought by changes in the surface composition (i.e., enrichment in Ni). Interestingly, although the surface Ni/Cu ratio of $Cu_{0.5}Ni_{0.5}$/MCM-48 is 1.08, this catalyst shows much lower activity compared to carbon-supported catalysts. Here, such a sharp decline in catalytic activity for $Cu_{0.5}Ni_{0.5}$/MCM-48 may be due to a stronger metal−silica interaction that could weaken the Cu−Ni interaction. To examine the metal−support

DOI: 10.1021/acscatal.5b00869
ACS Catal. 2015, 5, 5505−5511

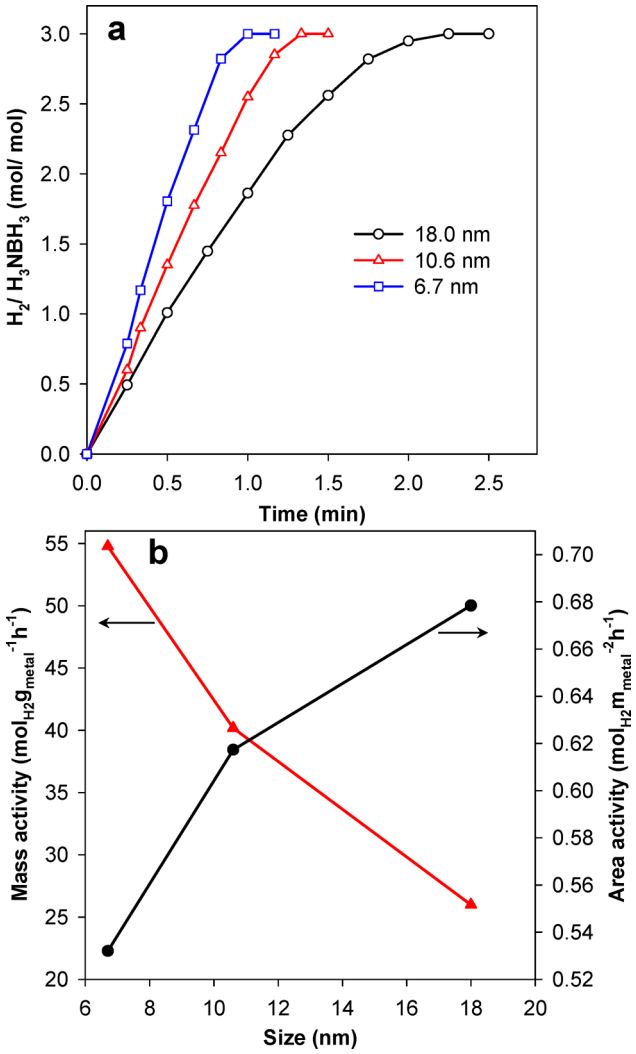

Figure 6. (a) Time course of hydrogen evolution from AB hydrolysis over $Cu_{0.5}Ni_{0.5}$/CMK-1 with different metal particle sizes. (b) Mass activity and area activity as a function of metal particle size in AB hydrolysis reaction catalyzed by $Cu_{0.5}Ni_{0.5}$/CMK-1 catalysts (T = 25 °C, Metal/AB = 0.072).

interaction, H_2-temperature-programmed reduction (H_2-TPR) of the silica-supported catalysts was performed (Figure S14). For comparison, TPR analyses of single metal silica-supported materials (i.e., Cu/MCM-48 and Ni/MCM-48) were also carried out. The resulting TPR profile of Cu/MCM-48 shows a single reduction peak at 201 °C, which can be attributed to the reduction of finely dispersed surface copper oxide species into copper. Meanwhile, a broad peak appears at 420 °C for Ni/MCM-48, corresponding to the reduction of nickel species in interaction with the silica support.[55,64] Note that the reduction of single bulk NiO occurs at 350 °C, suggesting that the strong Ni-silica interaction makes the nickel species more difficult to reduce. For the $Cu_{0.5}Ni_{0.5}$/MCM-48 catalyst, a reduction peak at 204 °C and a broad peak at around 400 °C can be assigned to the reduction of finely dispersed copper oxide species and nickel species closely interacting with the silica support, respectively. Thus, the presence of a strong interaction between nickel and silica could clearly impede the needed copper–nickel interaction, which plays a vital role in enhancing the catalyst reactivity.

CONCLUSIONS

In conclusion, we have presented the development of highly efficient nonprecious bimetallic supported CuNi catalysts using a simple incipient wetness with low-cost nitrate metal precursors. The above results reveal that composition, size of metal particle, and nature of support play critical roles in the activity and stability of the catalysts. The mesoporous carbon-spheres-supported bimetallic CuNi catalysts exhibit excellent performance in the catalytic hydrolysis of AB and catalytic decomposition of hydrous hydrazine with 100% H_2 selectivity. The metal particle sizes of the metal species can be controlled in the range from 6.7 to 18 nm with narrow size distribution on mesoporous carbon CMK-1 support simply by varying the metal loadings (5–20 wt %). The mass activity of the $Cu_{0.5}Ni_{0.5}$/CMK-1 catalyst was found to increase with decreasing metal particle size; however, the activity normalized to metal surface area declines slightly as the particle size decreases. Such observed size-dependent activity could be explained by modifications in surface composition as the particle size decreases. The $Cu_{0.5}Ni_{0.5}$/CMK-1 possessing an average metal particle size of 6.7 nm exhibits noticeably superior activity for dehydrogenation of AB with TOF as high as 3288 (mol_{H_2} mol_{metal}^{-1} h^{-1}) under ambient conditions, making it one of the best non-noble metal catalysts and even comparable to noble metal-based catalysts. The $Cu_{0.5}Ni_{0.5}$ supported on mesoporous MCM-48 silica nanospheres exhibits much lower activity for the AB hydrolysis reaction compared to carbon-supported counterparts mainly due to the strong nickel–silica interaction that could hinder the required Cu–Ni synergistic interaction. The observed high performance of the supported bimetallic CuNi nanocatalysts makes it possible to propose that the alloying of Cu and Ni leads to modification of the catalyst surface through intermetallic electronic interactions, which consequently improves substantially the reactivity of the metals.

Given that these two reactions are emerging as most promising approaches for chemical storage of hydrogen toward a hydrogen economy, the development of efficient and cost-effective catalysts, as well as knowledge about reactivity and selectivity of these reactions on nanocatalysts are of utmost importance. The present findings demonstrate that the optimum catalyst could be achieved through a combination of bimetallic effect along with tuning metal particle size and a proper choice of support.

ASSOCIATED CONTENT

Supporting Information

The Supporting Information is available free of charge on the ACS Publications website at DOI: 10.1021/acscatal.5b00869.

Detailed description of the materials syntheses and characterizations; additional EDS, TEM images, XRD profiles, XPS spectra, kinetic data, and tables presenting textural parameters (PDF)

AUTHOR INFORMATION

Corresponding Author

*E-mail: freddy.kleitz@chm.ulaval.ca.

Funding

This work was supported by NSERC (Canada) and FRQNT (Province of Quebec).

DOI: 10.1021/acscatal.5b00869
ACS Catal. 2015, 5, 5505–5511

Notes

The authors declare no competing financial interest.

■ ACKNOWLEDGMENTS

The authors thank Prof. Ryong Ryoo (KAIST, Korea) for the access to high-resolution transmission electron microscopy.

■ REFERENCES

(1) Studt, F.; Abild-Pedersen, F.; Bligaard, T.; Sorensen, R. Z.; Christensen, C. H.; Norskov, J. K. *Science* **2008**, *320*, 1320−1322.
(2) Huber, G. W.; Shabaker, J. W.; Dumesic, J. A. *Science* **2003**, *300*, 2075−2077.
(3) Ferrando, R.; Jellinek, J.; Johnston, R. L. *Chem. Rev.* **2008**, *108*, 845−910.
(4) Alonso, D. M.; Wettstein, S. G.; Dumesic, J. A. *Chem. Soc. Rev.* **2012**, *41*, 8075−8098.
(5) Park, J. Y.; Zhang, Y.; Grass, M.; Zhang, T.; Somorjai, G. A. *Nano Lett.* **2008**, *8*, 673−677.
(6) Norskov, J. K.; Bligaard, T.; Rossmeisl, J.; Christensen, C. H. *Nat. Chem.* **2009**, *1*, 37−46.
(7) Kim, D.; Resasco, J.; Yu, Y.; Asiri, A. M.; Yang, P. *Nat. Commun.* **2014**, *5*, 4948.
(8) Enache, D. I.; Edwards, J. K.; Landon, P.; Solsona-Espriu, B.; Carley, A. F.; Herzing, A. A.; Watanabe, M.; Kiely, C. J.; Knight, D. W.; Hutchings, G. J. *Science* **2006**, *311*, 362−365.
(9) Kaden, W. E.; Wu, T.; Kunkel, W. A.; Anderson, S. L. *Science* **2009**, *326*, 826−829.
(10) Nilsson, A.; Pettersson, L. G. M.; Norskov, J. K.; *Chemical bonding at surfaces and interfaces*; Elsevier: Netherlands, 2008.
(11) Prieto, G.; Beijer, S.; Smith, M. L.; He, M.; Au, Y.; Wang, Z.; Bruce, D. A.; de Jong, K. P.; Spivey, J. J.; de Jongh, P. E. *Angew. Chem., Int. Ed.* **2014**, *53*, 6397−6401.
(12) Acerbi, N.; Tsang, S. C. E.; Jones, G.; Golunski, S.; Collier, P. *Angew. Chem., Int. Ed.* **2013**, *52*, 7737−7741.
(13) Kobayashi, H.; Yamauchi, M.; Kitagawa, H.; Kubota, Y.; Kato, K.; Takata, M. *J. Am. Chem. Soc.* **2010**, *132*, 5576−5577.
(14) Campbell, C. T. *Nat. Chem.* **2012**, *4*, 597−598.
(15) Bruix, A.; Rodriguez, J. A.; Ramirez, P. J.; Senanayake, S. D.; Evans, J.; Park, J. B.; Stacchiola, D.; Liu, P.; Hrbek, J.; Illas, F. *J. Am. Chem. Soc.* **2012**, *134*, 8968−8974.
(16) Van Santen, R. A. *Acc. Chem. Res.* **2009**, *42*, 57−66.
(17) Wang, H.; Sapi, A.; Thompson, C. M.; Liu, F.; Zherebetskyy, D.; Krier, J. M.; Carl, L. M.; Cai, X.; Wang, L.-W.; Somorjai, G. A. *J. Am. Chem. Soc.* **2014**, *136*, 10515−10520.
(18) Boudart, M.; Djega-Mariadassou, G.; *Kinetics of heterogeneous catalytic reactions*; Princeton University Press: Princeton, NJ, 1984.
(19) Shi, J. *Chem. Rev.* **2013**, *113*, 2139−2181.
(20) Campbell, C. T. *Acc. Chem. Res.* **2013**, *46*, 1712−1719 s.
(21) An, K.; Alayoglu, S.; Musselwhite, N.; Plamthottam, S.; Melaet, G.; Lindeman, A. E.; Somorjai, G. A. *J. Am. Chem. Soc.* **2013**, *135*, 16689−16696.
(22) Hu, P.; Huang, Z.; Amghouz, Z.; Makkee, M.; Xu, F.; Kapteijn, F.; Dikhtiarenko, A.; Chen, Y.; Gu, X.; Tang, X. *Angew. Chem., Int. Ed.* **2014**, *53*, 3418−3421.
(23) Kozlov, S. M.; Neyman, K. M. *Top. Catal.* **2013**, *56*, 867−873.
(24) Zhu, X.; Cho, H.-R.; Pasupong, M.; Regalbuto, J. R. *ACS Catal.* **2013**, *3*, 625−630.
(25) Farmer, J. A.; Campbell, C. T. *Science* **2010**, *329*, 933−936.
(26) Yeung, C. M. Y.; Yu, K. M. K.; Fu, Q. J.; Thompsett, D.; Petch, M. I.; Tsang, S. C. *J. Am. Chem. Soc.* **2005**, *127*, 18010−18011.
(27) Munnik, P.; de Jongh, P. E.; de Jong, K. P. *J. Am. Chem. Soc.* **2014**, *136*, 7333−7340.
(28) Che, M. In *Advances in Catalysis*; Eley, D. D., Pines, H., Weisz, P. B., Eds.; Elsevier: Amsterdam, 1989; Vol. *36*, pp 55−172.
(29) Schlapbach, L.; Zuttel, A. *Nature* **2001**, *414*, 353−358.
(30) Stephens, F. H.; Pons, V.; Baker, R. T. *Dalton Trans.* **2007**, *25*, 2613−2626.
(31) Yang, J.; Sudik, A.; Wolverton, C.; Siegel, D. J. *Chem. Soc. Rev.* **2010**, *39*, 656−675.
(32) Sanyal, U.; Demirci, U. B.; Jagirdar, B. R.; Miele, P. *ChemSusChem* **2011**, *4*, 1731−1739.
(33) Yadav, M.; Xu, Q. *Energy Environ. Sci.* **2012**, *5*, 9698−9725.
(34) Singh, S. K.; Xu, Q. *Catal. Sci. Technol.* **2013**, *3*, 1889−1900.
(35) Sun, D.; Mazumder, V.; Metin, O.; Sun, S. *ACS Nano* **2011**, *5*, 6458−6464.
(36) Zhu, Q.-L.; Li, J.; Xu, Q. *J. Am. Chem. Soc.* **2013**, *135*, 10210−10213.
(37) Singh, S. K.; Singh, A. K.; Aranishi, K.; Xu, Q. *J. Am. Chem. Soc.* **2011**, *133*, 19638−19641.
(38) Hu, J.; Chen, Z.; Li, M.; Zhou, X.; Lu, H. *ACS Appl. Mater. Interfaces* **2014**, *6*, 13191−13200.
(39) Singh, S. K.; Xu, Q. *Inorg. Chem.* **2010**, *49*, 6148−6152.
(40) Chen, G.; Desinan, S.; Rosei, R.; Rosei, F.; Ma, D. *Chem. Commun.* **2012**, *48*, 8009−8011.
(41) Yamada, Y.; Yano, K.; Fukuzumi, S. *Energy Environ. Sci.* **2012**, *5*, 5356−5363.
(42) Manukyan, K. V.; Cross, A.; Rouvimov, S.; Miller, J.; Mukasyan, A. S.; Wolf, E. E. *Appl. Catal., A* **2014**, *476*, 47−53.
(43) Yen, H.; Kleitz, F. *J. Mater. Chem. A* **2013**, *1*, 14790−14796.
(44) Yan, J.-M.; Wang, Z.-L.; Wang, H.-L.; Jiang, Q. *J. Mater. Chem.* **2012**, *22*, 10990−10993.
(45) (a) Yamada, Y.; Yano, K.; Xu, Q.; Fukuzumi, S. *J. Phys. Chem. C* **2010**, *114*, 16456−16462. (b) Kaya, M.; Zahmakiran, M.; Ozkar, S.; Volkan, M. *ACS Appl. Mater. Interfaces* **2012**, *4*, 3866−3873.
(46) He, L.; Huang, Y.; Wang, A.; Wang, X.; Chen, X.; Delgado, J. J.; Zhang, T. *Angew. Chem., Int. Ed.* **2012**, *51*, 6191−6194.
(47) Wang, S.; Zhang, D.; Ma, Y.; Zhang, H.; Gao, J.; Nie, Y.; Sun, X. *ACS Appl. Mater. Interfaces* **2014**, *6*, 12429−12435.
(48) Xu, Q.; Chandra, M. *J. Alloys Compd.* **2007**, *446-447*, 729−732.
(49) (a) Can, H.; Metin, O. *Appl. Catal., B* **2012**, *125*, 304−310. (b) Yan, J.-M.; Zhang, X.-B.; Akita, T.; Haruta, M.; Xu, Q. *J. Am. Chem. Soc.* **2010**, *132*, 5326−5327.
(50) Metin, O.; Mazumder, V.; Ozkar, S.; Sun, S. *J. Am. Chem. Soc.* **2010**, *132*, 1468−1469.
(51) (a) Li, P.-Z.; Aijaz, A.; Xu, Q. *Angew. Chem., Int. Ed.* **2012**, *51*, 6753−6756. (b) Yan, J.-M.; Zhang, X.-B.; Han, S.; Shioyama, H.; Xu, Q. *Angew. Chem., Int. Ed.* **2008**, *47*, 2287−2289. (c) Cao, C.-Y.; Chen, C.-Q.; Li, W.; Song, W.-G.; Cai, W. *ChemSusChem* **2010**, *3*, 1241−1244. (d) Zahmakıran, M.; Durap, F.; Özkar, S. *Int. J. Hydrogen Energy* **2010**, *35*, 187−197.
(52) (a) Chandra, M.; Xu, Q. *J. Power Sources* **2006**, *156*, 190−194. (b) Chandra, M.; Xu, Q. *J. Power Sources* **2007**, *168*, 135−142.
(53) Wu, C.-T.; Qu, J.; Elliott, J.; Yu, K. M. K.; Tsang, S. C. E. *Phys. Chem. Chem. Phys.* **2013**, *15*, 9043−9050.
(54) Studt, F.; Abild-Pedersen, F.; Wu, Q.; Jensen, A. D.; Temel, B.; Grunwaldt, J.-D.; Norskov, J. K. *J. Catal.* **2012**, *293*, 51−60.
(55) Lin, J.-H.; Guliants, V. V. *ChemCatChem* **2012**, *4*, 1611−1621.
(56) Chen, L.-C.; Lin, S. D. *Appl. Catal., B* **2011**, *106*, 639−649.
(57) Lin, J.-H.; Biswas, P.; Guliants, V. V.; Misture, S. *Appl. Catal., A* **2010**, *387*, 87−94.
(58) Naghash, A. R.; Etsell, T. H.; Xu, S. *Chem. Mater.* **2006**, *18*, 2480−2488.
(59) Gan, L.-Y.; Tian, R.-Y.; Yang, X.-B.; Lu, H.-D.; Zhao, Y.-J. *J. Phys. Chem. C* **2012**, *116*, 745−752.
(60) Kaneda, M.; Tsubakiyama, T.; Carlsson, A.; Sakamoto, Y.; Ohsuna, T.; Terasaki, O.; Joo, S. H.; Ryoo, R. *J. Phys. Chem. B* **2002**, *106*, 1256−1266.
(61) Shin, H. J.; Ryoo, R.; Liu, Z.; Terasaki, O. *J. Am. Chem. Soc.* **2001**, *123*, 1246−1247.
(62) Kim, T.-W.; Chung, P.-W.; Lin, V. S. Y. *Chem. Mater.* **2010**, *22*, 5093−5104.
(63) Ertl, G.; Knözinger, H.; Schüth, F.; Weitkamp, J. *Handbook of Heterogeneous Catalysis*, Vol. *1*; Wiley: Berlin, 2008.
(64) Yin, A.; Wen, C.; Guo, X.; Dai, W.-L.; Fan, K. *J. Catal.* **2011**, *280*, 77−88.

DOI: 10.1021/acscatal.5b00869
ACS Catal. 2015, 5, 5505−5511